Supporting Information

Wei et al. 10.1073/pnas.1418494112

SI Materials and Methods

Materials. Doxorubicin hydrochloride was purchased from Beijing Huafeng United Technology Co., Ltd. Caelyx was obtained from the pharmacy of Institut Paoli-Calmettes. The 3-(4,5-dimethylthiazol-2-yl)-2,5-diphenyltetrazolium bromide (MTT), chlorpromazine, cytochalasin D, and genistein were purchased from Sigma-Aldrich. Hoechst 34580, LysoSensor Green, DiR, and APC Annexin V/Dead Cell Apoptosis Kit with APC Annexin V and SYTOX Green for Flow Cytometry were purchased from Life Technologies. All other reagents were analytic grade and used without further purification.

Preparation of Doxorubicin-Loaded Nanomicelles. The AmDM was used to encapsulate doxorubicin via film dispersion method (1). Doxorubicin hydrochloride (ranging from 1.2 to 3.2 mg) was dissolved in 1.0 mL mixed solvent (chloroform:methanol = 3:2, vol/vol), adding triethylamine (molar ratio of doxorubicin: triethylamine = 1:3) to obtain hydrophobic doxorubicin. The drug was then mixed with 3 mg of AmDM in 3.0 mL of mixed solvent at different mass ratios (15:6, 15:8, 15:10, and 15:16). The solvent was removed by vacuum rotary evaporation to form a dry film. The dried film was then hydrated with Hepes buffer (10 mM, pH 7.4) at 60 °C for 30 min under stirring. Nonencapsulated doxorubicin was separated by filtration through a 0.45-μm polycarbonate membrane (Millipore Co.) followed by dialysis for 9 h (changing water every hour) using a membrane with molecular weight cutoff of 2,000 Da. The product in the dialysis tube was subsequently lyophilized. The amount of doxorubicin encapsulated in the micelles was measured using a fluorospectrophotometer with excitation wavelength at 477 nm and emission wavelength at 591 nm. Blank AmDM micelles were prepared using the same procedures without doxorubicin addition.

The drug-loading content and drug encapsulation efficiency were calculated as below:

$$\text{drug loading content } (\%) = \mathrm{W}_t/\mathrm{W}_s \times 100\%$$

$$\text{encapsulation efficiency } (\%) = \mathrm{W}_t/\mathrm{W}_o \times 100\%.$$

W_t represents the amount of doxorubicin that loaded into nanoparticles; W_o represents the initial amount of doxorubicin fed; W_s represents the amount of nanoparticles after lyophilization.

Critical Micelle Concentration of AmDM. The critical micelle concentration of AmDM was assessed using pyrene as the fluorescent probe. A serial AmDM solutions ranging from 1.2×10^{-7} to 5.0×10^{-4} mol/L was prepared. Then the solutions were added to flasks containing the fluorescent probe pyrene, respectively, with the final concentration of pyrene being 6.0×10^{-7} M in water. The solutions were then sonicated for 30 min and kept for 2 h at room temperature to finalize the micelle formation. Next, the fluorescent spectra were measured at the excitation wavelength of 335 nm on a fluorescence spectrophotometer (F-4500; Hitachi). Excitation and emission bandwidths were 5 nm. The fluorescent intensity ratio of I_{373}/I_{384} was analyzed as a function of logarithm AmDM concentration.

Physicochemical Properties of Nanomicelles. The size and morphology of AmDM and AmDM/DOX nanomicelles were obtained using a TEM (HT7700; Hitachi). Briefly, 25 μM of each sample was prepared in water and then 5.0 μL of each sample was dropped onto the copper grids and air-dried at 42 °C. Then the grids were stained with 1% (wt/vol) uranyl acetate solution for 30 s before taking images. The size distribution of AmDM and AmDM/DOX nanomicelles was determined by DLS using Zetasizer Nano-ZS (Malvern, Ltd.) with a He-Ne ion laser of 633 nm.

Computational Methodology. In this work we adopted a multiscale molecular simulations strategy based on the systematic elimination of computationally expensive degrees of freedom characterizing lower-scale molecular simulations (e.g., atomistic molecular dynamics simulations) while retaining implicitly their influence on the remaining degrees freedom at higher-scale simulations (e.g., mesoscopic simulations). According to this methodology, using the information obtained from atomistic MD simulation, we parameterized the DPD (2) models so as to incorporate all essential physics/phenomena observed at the finer level. The outline of the general strategy of our multiscale modeling approach may be summarized as follows: (*i*) extensive explicit solvent atomistic MD calculations were performed on model compounds (AmDM and DOX) to derive important interactions/correlations, which were then used to parameterize the mesoscale models; (*ii*) derivation of DPD parameters the exploiting energetical, conformational, and structural properties obtained from MD simulation at point *i*). Langevin dynamics were then conducted using the DPD representation of the system, where the elementary unit (called "bead") is a spherical particle representing a fluid element, which can contain a number of solvent molecules, drug, or amphiphilic dendrimer segments.

Film dispersion simulation. In our pursuit to properly mimic AmDM self-assembly process, we simulated micelle formation via solvent evaporation at the mesoscale level. The effect of solvent evaporation was reproduced in the DPD framework according to the procedure proposed by Neratova et al. (3). Briefly, the AmDM or AmDM/DOX solution was placed on an impenetrable, fixed, noninteracting substrate (4). At the top of the film phase, a gas phase and an exchange phase were created. During the DPD simulations, when solvent particles leave the film phase and appear in the exchange region, they are transformed into gas particles. As a result of such process, the fraction of the gas phase increases, and the thickness of the film decreases. Gas and polymer phases were assumed to be immiscible.

Unless otherwise stated, in all DPD studies the following reduced units were used: r_c is the unit of length, m is the mass of a DPD particle, and kT is the unit of energy. Simulations were carried out at a total particle density of $\rho = 3$ in a box of $40 \times 40 \times 60$ with a time step of $\Delta t = 0.04$ and a simulation period of 1×10^5 steps or longer until stable morphology was observed. Calculations were performed using the commercial package Materials Studio 5.0 (Accelrys Inc.) taking advantage of its scripting capabilities.

The molecular structure of AmDM in the DPD representation is divided into five types of beads: a neutral bead, type C, identifies the hydrophobic chain building block, and two bead types (RT and R) represent the terminal and branch unit of the AmDM dendron, respectively. Two further bead types—G, linking the hydrophilic and hydrophobic parts together, and L, representing the dendron focal point—were also used. The DOX model features a linear bead–spring chain representation, where a bead type D1 represents the aromatic fraction, a bead of type D2 the cycloaliphatic portion, and a bead of type D3 the remaining, polar moiety. Solvent molecules (chloroform and methanol), inert substrate, and gas were simulated by single bead types (Ch, Me, S, and Gs, respectively). The mesoscale topology of AmDM

and DOX molecules described above was derived through a multiscale approach (points *i* and *ii* above) exploiting the comparison of the appropriate MD and DPD pair–pair correlation functions of each compound in solution, according to a procedure validated by our group on related and/or self-assembling compounds (5–8).

Intra- and intermolecular interactions between DPD particles are expressed by a conservative, soft-repulsive force, vanishing beyond a certain cutoff radius r_c, whose value sets the unit length in simulations. The intensity of this conservative force is defined by a pair-repulsive parameter a_{ij}, which accounts for the underlying chemistry of the system considered. In this work, we used a well-validated strategy that correlates the interaction energies estimated from atomistic MD simulations to the mesoscale a_{ij} parameter values (9–11). Following this computational recipe, the atomistic interaction energies between the components of the solvated AmDM/DOX systems were estimated using the MM/PBSA technique (12) as implemented in the Amber 14 package (13). The corresponding MD trajectories were obtained running the simulations on the EURORA GPU-CPU cluster (CINECA, Bologna, Italy). The AmDM and DOX models were built, parameterized, and optimized following a consolidated procedure described in details in our previous work (14–16). Then, the AmDM/DOX structure was solvated in a chloroform/methanol box to generate a bulk system at a concentration lower than the corresponding experimental CMC value. The solvated molecules were subjected to a combination of steepest descent/conjugate gradient minimization of the potential energy, during which all bad contacts were relieved. The relaxed systems were then gradually heated to 300 K in three intervals by running constant volume-constant temperature (NVT) MD simulation, allowing a 0.5-ns interval per 100 K. Subsequently, 10-ns MD simulations under isobaric–isothermal (NPT) conditions were conducted to fully equilibrate each solvated compound. Temperature control was achieved using the Andersen temperature coupling scheme (17) and an integration time step of 2 fs. At this point, these MD runs were followed by other 20 ns of NVT MD collection runs. Energetic data were gathered from the last equilibrated 10 ns of the production runs. The particle-mesh Ewald method (18) was used to treat the long-range electrostatics with a direct space cutoff of 10 Å. To calculate interaction energies and conformational properties, 1,000 snapshots were saved during the MD data collection period described above, one snapshot per 10 ps of MD simulation.

Once obtained, the atomistic interaction energies were rescaled onto the corresponding mesoscale segments adapting the procedure described in detail in refs. 19 and 20. The self-repulsive interaction parameters for chloroform and methanol were set equal to $a_{ChCh} = 18$ and $a_{MeMe} = 26$ based on the direct relationship with their isothermal compressibility (21, 22). Once these parameters were assigned, all of the remaining bead–bead interaction parameters for the DPD simulations were easily obtained, starting from the atomistic interaction energies values.

AmDM and AmDM/DOX micelles in solution. DPD AmDM and AmDM/DOX micelles as obtained from film deposition simulations were then solvated in a cubic 3D periodic water box. Both systems were equilibrated for at least 1×10^6 steps before performing postprocessing analysis. The DPD interaction parameters a_{ij} were derived repeating the same multiscale protocol described above in aqueous solution. A TIP3P model (23) was chosen to represent water molecules in our MD calculations, and a single bead type W was used to model water molecules at the mesoscale level. The bead–bead interaction parameter for water was set equal to $a_{WW} = 25$ in agreement with the assumed value of DPD density $\rho = 3$ (2). The maximum level of hydrophobic/hydrophilic repulsion was captured by setting the interaction parameter a_{ij} between the water bead W and the hydrocarbon tail bead C as 82.

In Vitro Drug Release. The release of doxorubicin from AmDM/DOX nanoparticles was performed using dialysis method (24) with dialysis membrane tubes (molecular weight cutoff: 12,251 Da). Briefly, the AmDM/DOX solution (DOX equivalent of 250 μg) was dispersed in 10 mM PBS at different pH value (pH 7.4 and pH 5.0) and then transferred to dialysis membrane tubes. These tubes were immersed into 35 mL of PBS solution with different pH value and shaken at 37 °C for 0.5, 1, 2, 4, 6, 8, 10, 12, and 24 h. At each time point, 1.0 mL of the external buffer was collected and replaced by 1.0 mL of fresh buffer. The doxorubicin concentration was measured using a fluorospectrophotometer with excitation wavelength at 477 nm and emission wavelength at 591 nm.

pH Titration Experiment. A solution of AmDM (2.0 mmol in 10 mL) was adjusted to pH 2–3 using 0.50 M HCl, then the pH titration curve was recorded by adding 0.10 M NaOH into the solution using Mettler Toledo 320-S pH meter (25).

Cell Culture. Doxorubicin-sensitive and -resistant breast cancer cell lines (MCF-7S and MCF-7R) were generously provided by R. Tang, Service d'Hématologie Clinique et de Thérapie Cellulaire, Hôpital St Antoine, Paris. Human castration-resistant prostate cancer PC-3 cells, human hepatoma HepG2 cells, and human cervical cancer HeLa cells were purchased from the American Type Culture Collection (LGC Standards SARL). Cell culture medium RPMI 1640 and DMEM, MEM nonessential amino acids, Hepes, and ANTI–ANTI were purchased from Life Technologies. MCF-7S and MCF-7R cells were maintained in RPMI medium 1640 containing 10% FBS (Lonza Group Ltd.), insulin Humalog, MEM nonessential amino acids, Hepes, and ANTI–ANTI. PC3 cells and HeLa cells were cultured in DMEM containing 10% FBS. HepG2 cells were cultured in RPMI medium 1640 containing 10% FBS. All cells were cultured at 37 °C in humidified atmosphere containing 5% CO_2.

Drug Penetration Study in 3D-Cultured Tumor Spheroids. Multicellular tumor spheroids were constructed with MCF-7R cells using the reported protocol (26). Agarose solution (0.8%, wt/vol) was prepared in Milli-Q water by heating at 90 °C for 15 min. Each well of the 96-well plates was coated with 50 μL of the agarose solution, and then UV irradiation for 30 min for sterilization. Next, 100-μL cell suspensions containing 500 MCF-7R cells were seeded into the agarose-coated 96-well plates. The medium was changed every 2 d for 1 wk to form the tumor spheroids.

To evaluate the drug penetration ability, the MCF-7R spheroids were incubated with free DOX or AmDM/DOX nanomicelles at a doxorubicin concentration of 10 μM for 4 h. Then the tumor spheroids were washed with PBS twice and fixed by 4% (wt/vol) formaldehyde solution for 20 min, followed by further washing three times. The fixed spheroids were transferred to confocal dishes and analyzed using two-photon microscope (Carl Zeiss LSM7MP). Z-stack images were obtained by scanning the tumor spheroids step by step with 10 μm thickness. This experiment was performed at the PiCSL-France-BioImaging core facility (Institut de Biologie du Développement de Marseille, Aix-Marseille Université), a member of the France-BioImaging national research infrastructure.

In Vitro Anticancer Activity Assay. The antiproliferation activities of the free anticancer drug DOX, the clinical nanodrug Caelyx, and the AmDM/DOX micelles against human breast cancer cells (MCF-7S and MCF-7R), human prostate cancer cells (PC3), human cervical cancer cells (HeLa cells), and human hepatoma cells (HepG2 cells) were evaluated using a microculture tetrazolium (MTT) method. MCF-7S, MCF-7R, HeLa, and PC3 cells (5.0×10^3 cells per well) and HepG2 cells (1.0×10^4 cells per well) were seeded in 96-well plates, respectively, and incubated overnight to adhere. Then the cells were incubated with free

DOX, Caelyx, and AmDM/DOX at serial doxorubicin concentrations ranging from 0.001 to 100 μM for 24 h, followed by replacing with 100 μL 1.0 mg/mL MTT solution and incubated for another 3 h. Cells treated with complete medium were used as control. Then the medium was replaced with 100 μL DMSO solution. After 10-min shaking, the absorbance was measured at 595 nm wavelength using a microplate reader (Tecan). All of the experiments were carried out in triplicate.

Cell Apoptosis Assay. MCF-7R cells were planted into six-well plates at a density of 1.0×10^5 cells per well and cultured for 24 h. Then the culture medium was replaced with free DOX, blank AmDM micelles, or AmDM/DOX micelles at a doxorubicin concentration of 10 μM in complete medium. Cells with no treatment were used as control. After 15 h incubation at 37 °C, the cells were harvested, washed, and resuspended with 100 μL 1× Annexin-binding buffer. Subsequently, 5.0 μL APC Annexin V solution and 1.0 μL of the 1.0 μM SYTOX Green stain working solution were added into the cell suspension and incubated at 37 °C for 15 min under protection from light. The apoptosis assay was then analyzed using flow cytometry (LSRII; Becton Dickinson).

Internalization of Free DOX and AmDM/DOX Nanomicelles. The cell internalization of free DOX and AmDM/DOX was examined in MCF-7S and MCF-7R cells using fluorescence-activated cell sorting. Briefly, 1.5×10^5 cells per well were seeded into six-well plates and incubated at 37 °C overnight. Then the medium was removed and replaced with free DOX and AmDM/DOX micelles at a final concentration of 2.0 μM and 4.0 μM for 30 min and 2 h under 37 °C. Afterward, the cells were harvested and washed with 1× PBS solution three times and then analyzed by flow cytometry using FACSCanto II Flow Cytometer (Becton Dickinson). Each assay was performed in triplicate.

The cellular uptake of free DOX and AmDM/DOX was detected in MCF-7R cells using confocal microscope. Briefly, 1.5×10^4 cells per well were seeded into confocal dishes and incubated at 37 °C overnight. Then the medium was removed and replaced with solutions of free DOX and AmDM/DOX micelles, respectively, at a final concentration of 10 μM DOX under 37 °C. After 10 h incubation, the cells were fixed using 4% (wt/vol) formaldehyde solution for 15 min, followed by Hoechst 34580 staining to the nuclei, and then imaging using a Zeiss confocal microscope (LSM 510 META).

Subcellular Localization of Free DOX and AmDM/DOX. MCF-7R cells were seeded into 3.5-cm confocal dishes and cultured at 37 °C for 24 h, then the cells were incubated with free DOX or AmDM/DOX nanomicelles at a doxorubicin concentration of 10 μM for 4 h at 37 °C. Cells with no treatment were used as control. Next, the medium was removed and washed with PBS solution twice, followed by staining with LysoSensor Green (1:1,000 diluted in PBS) for another 15 min. Hoechst 34580 (1:2,000, diluted in PBS) was used to stain the nucleus. Then the subcellular distribution of doxorubicin was recorded using a Zeiss confocal microscope (LSM510 META).

Endocytotic Mechanism of AmDM/DOX Nanomicelle. To investigate the possible endocytosis mechanism of AmDM/DOX nanomicelles, assays of specific inhibition on endocytosis pathways were evaluated using MCF-7R cells, with nontreatment as control. MCF-7R cells were planted at a density of 1.0×10^5 cells per well in the 12-well plates and incubated in complete medium for 24 h. The cells were then washed with PBS twice, followed by preincubating at 37 °C for 1 h with one of the following endocytosis inhibitors dissolved in serum-free RPMI medium 1640: chlorpromazine (an endocytotic inhibitor of clathrin-mediated endocytosis), cytochalasin D (an endocytotic inhibitor of macropinocytosis-mediated endocytosis), or genistein (an endocytotic inhibitor of caveolae-mediated endocytosis). Next, the medium was removed and replaced with complete RPMI medium 1640 containing AmDM/DOX at doxorubicin concentration of 2.0 μM and different inhibitors for another 15 min. After that, the medium was removed and the cells were washed twice with cold PBS solution. The cells were then collected and analyzed by flow cytometry. All experiments were carried out in triplicate.

Drug Efflux Inhibition of AmDM/DOX. To determine the potential drug efflux inhibitory effect of AmDM/DOX nanomicelles, we evaluated the drug efflux of free DOX and AmDM/DOX nanomicelles in efflux pumps (P-gp protein) overexpressing MCF-7R cells. The 1.5×10^5 cells per well were seeded into six-well plates and incubated at 37 °C overnight. The cells were incubated either with 10 μM free DOX or AmDM/DOX nanomicelles for 4 h. Then the medium was removed and the cells were washed twice with PBS solution, and subsequently incubated with fresh complete medium for different time intervals (0, 1, 3, 6, or 8 h). At the end of incubation time, the cells were washed, harvested, and analyzed using an Attune acoustic focusing cytometer (Applied Biosystems, Life Technologies). All experiments were carried out in triplicate.

Animal Experiments. Research involving animals was approved by the Ethical Committee of the Bouche du Rhône prefecture in France and the institutional Animal Care and Use Committee of Peking University in China. Dr. P. Rocchi possesses authorized agreement (A13-477) for animal handling and experimentation for this study in France. Female NSG mice were provided by Centre de Recherche en Cancérologie de Marseille, and male C57BL/6 mice were purchased from the Academy of Military Medical Sciences of China. NSG mice were maintained in an agreed animal facility (agreement no. 13.2700) in Marseille and C57BL/6 mice in Peking University Laboratory Animal Center (an Association for Assessment and Accreditation of Laboratory Animal Care International-accredited experimental animal facility). All mice were fed under specific pathogen-free conditions and handled according to the principles of the laboratory animal care and recommendations to ethics laws.

Hemolysis Experiment. Red blood cells were isolated from 1 mL of fresh blood collected from healthy female NSG mice by centrifuging at $10{,}000 \times g$ for 5 min. The red blood cells (RBCs) were then washed several times with PBS buffer until no color was seen in the supernatant. RBCs were then suspended in 15 mL PBS, and 0.50 mL of such RBC suspension was added to 0.50 mL of suspension containing different concentrations of AmDM micelles at 2.5, 5.0, 10, 20, 40, and 80 μg/mL in PBS buffer to offer the final concentrations of 1.3, 2.5, 5.0, 10, 20, and 40 μg/mL, respectively. A 0.50-mL RBC suspension incubated with 0.50 mL PBS or 0.50 mL distilled water was used as negative and positive controls, respectively. The samples were mixed gently, left at room temperature for 2 h, and then centrifuged at $10{,}000 \times g$ for 5 min. A total of 100 μL of supernatant was transferred to a 96-well plate and the absorbance of hemoglobin at 540 nm was measured. The percentage of hemolysis was calculated as follows:

$$\text{hemolysis } \% = [(\text{sample absorbance} - \text{negative control})/(\text{positive control} - \text{negative control})] \times 100\%.$$

In Vivo Anticancer Activity Assay. The 1.0×10^7 MCF-7R cells suspended in 100 μL of PBS buffer/Matrigel (BD Pharmingen) mixed solution (1:1, vol/vol) were inoculated s.c. in the flank region of 5-wk-old female NSG mice. When the tumor size reached ~50 mm^3, the female NSG mice were treated with free DOX and AmDM/DOX at a doxorubicin dose of 2.5 mg/kg and 5.0 mg/kg by tail vein injection twice per week five times ($n = 7$

per group). PBS and empty AmDM groups were used as control (n = 7 per group). The mouse body weights were recorded to evaluate the toxicity. Tumor volume was measured twice per week using a caliper in two dimensions and calculated using the following formula: volume = $1/2 \times LW^2$ (L is the longest diameter and W is the shortest diameter of the tumor). At the end, all of the organs were taken out, followed by making paraffin sections. The paraffin sections of all of the tumors were stained by anti–K_i-67 monoclonal antibody to evaluate the tumor proliferation; the paraffin sections of all of the organs were performed with HES staining for histological analysis (27).

Immunohistochemistry. Three-micrometer paraffin sections of tumors were dried overnight at room temperature. Before antibody staining, the slides were first incubated for 1.5 h at 65 °C, then incubated for 20 min at 95 °C with EnVision FLEX Target Retrieval Solution (low pH, pH 6) (K8005; Dako UK Ltd.), followed by pretreating with Epitope Retrieval Solution (containing detergent; K5207; Dako UK Ltd.) for 30 min at room temperature to unmask binding epitopes. After blocking of endogenous peroxidase activity with Dako EnVision FLEX Peroxidase-Blocking Reagent SM801 (ready to use) (K8000, K8002, K8023; Dako UK Ltd.) for 5 min, the slides were washed thoroughly in wash buffer FLEX (Dako UK Ltd.). After one wash in wash buffer FLEX, the slides were incubated with a FLEX Monoclonal Mouse Anti-Human K_i-67 Antigen clone MIB-1 (IR62; Dako UK Ltd.) for 1 h at room temperature. After two more washes in wash buffer FLEX, Dako EnVision FLEX/HRP SM802 (K8000; Dako UK Ltd.) was added for 20 min at room temperature. Then a series of two washing with wash buffer FLEX, the staining was visualized by adding diaminobenzidine (Dako UK Ltd.) for 10 min at room temperature. The slides were washed well in wash buffer FLEX and counterstained with EnVision FLEX HEMATOXILIN SM806 (K8008; Dako UK Ltd.) for 5 min, then washed once with wash buffer FLEX and a second time with water, and then dehydrated, cleared, and mounted with aqueous mounting media (Aquatex 108562; Merck Chimie SAS). Positive and negative controls were performed with each batch of slides. Photomicrographs were taken through a Nikon eclipse E400 microscope (Nikon France SA) coupled to a QICAM Fast 1394 digital camera (QImaging; Roper Engineering) (28).

HES Staining. Four-micrometer paraffin sections of different organs were incubated 40 min at 95 °C, then slides were deparaffinized twice in histolemon (45491; Carlo Erba reagent) for 10 min and then rehydrated with 100% ethanol for 6 min and 95% (vol/vol) ethanol for 5 min. After rinsing in tap water for 3 min, then in distilled water for 2 min, the slides were stained with Mayer's acid hematoxylin (FR09381; Biolyon) for 5 min. After washing in tap water for 2 min, the sections were differentiated with Phloxine B (361470; RAL Diagnostics) for 30 s After washing in running tap water for 2 min and another three dips in 100% ethanol for 2, 1, and 1 min, respectively, the slides then were stained in safran (food powder) for 7 min. After dehydration and differentiation in 100% ethanol for 30 s twice, the slides were cleared in histolemon twice and mounted with aqueous mounting media (Aquatex 108562; Merck Chimie SAS). Photomicrographs were taken through a Nikon eclipse E400 microscope (Nikon France SA) coupled to a QICAM Fast 1394 Digital Camera (QImaging; Roper Engineering) (28).

In Vivo Biodistribution. AmDM/DiR nanomicelles were prepared using the same method described above. Briefly, 25 μg of DiR was dissolved in 1.0 mL mixed solvent (chloroform: methanol = 3:2, vol/vol), then the DiR solution was mixed with AmDM in 3.0 mL of mixed solvent. The solvent was removed by vacuum rotary evaporation to form a dry film. Then the dried film was hydrated with Hepes buffer (10 mM, pH 7.4) at 60 °C for 30 min under stirring. Nonencapsulated DiR was separated by filtration through a 0.45-μm polycarbonate membrane (Millipore Co.), followed by dialysis for 9 h (changing water every hour) using a membrane with molecular weight cutoff of 2,000 Da.

To determine the in vivo biodistribution, female NSG mice bearing MCF-7R tumors were injected with 100 μL of PBS, free DiR and AmDM/DiR nanomicelles i.v. at a dose corresponding to 8.0 μg/mL of DiR via tail vein (n = 4 per group). The real-time distribution and tumor accumulation of PBS, free DiR, and AmDM/DiR nanomicelles were recorded at 0.5, 2, 8, 12, 24, and 48 h postinjection using an in vivo imaging system (Photon Imager; Biospace Lab).

In Vivo Tumor Penetration. Female NSG mice bearing MCF-7R tumors were injected with 100 μL of free DOX and AmDM/DOX i.v. at a doxorubicin dose of 15 mg/kg via tail vein; PBS group was used as control. After 12 h, the tumors were excised from the mice and embedded in optimal cutting temperature compound and cut into 10-μm slides. Tumor vessels in the frozen tumor section were stained using FITC-tagged CD31 antibody. Briefly, the sections were fixed in 4% (wt/vol) formaldehyde solution for 20 min, washed three times in PBS, followed by blocking with 10% (wt/vol) BSA for 1 h, then incubated with rat anti-CD31 (1:50 dilution, 550274; BD Pharmingen) antibody overnight at 4 °C. Sections were then washed with PBS three times and stained with a FITC-conjugated goat anti-rat IgG secondary antibody (1:100, sc-2011; Santa Cruz Biotechnology, Inc.) for 1 h. The sections were then washed, covered with coverslip, and observed using a Zeiss LSM510 confocal microscope.

In Vivo Toxicity. To assess the in vivo toxicity of AmDM nanocarriers, 6- to 8-wk-old male C57BL/6 mice were injected once i.v. with PBS buffer or AmDM nanocarriers (15 mg/kg; n = 5). After 3 h, mice were killed and the plasma samples were collected. Two indicators measuring the hepatic enzyme level, ALT and gamma glutamyl transferase; two indicators monitoring the kidney function, creatinine and blood urea nitrogen; and the cholesterol level in the blood were evaluated using SABA-18 Automatic Biochemical Analyzer (Analyzer Medical System) (25).

1. Wei T, et al. (2013) Functionalized nanoscale micelles improve drug delivery for cancer therapy in vitro and in vivo. *Nano Lett* 13(6):2528–2534.
2. Groot RD, Warren PB (1997) Dissipative particle dynamics: Bridging the gap between atomistic and mesoscopic simulation. *J Chem Phys* 107(11):4423–4435.
3. Neratova IV, Pavlov AS, Khalatur PG (2010) Effect of a solvent on self-organization in nanofilms: Modeling by the dissipative particle dynamics method. *Polym Sci Ser A* 52(9):959–969.
4. Toth R, et al. (2009) Multiscale computer simulation studies of water-based montmorillonite/poly(ethylene oxide) nanocomposites. *Macromolecules* 42(21):8260–8270.
5. Liu X, et al. (2011) Structurally flexible triethanolamine core PAMAM dendrimers are effective nanovectors for DNA transfection in vitro and in vivo to the mouse thymus. *Bioconjug Chem* 22(12):2461–2473.
6. Barnard A, et al. (2014) Double-degradable responsive self-assembled multivalent arrays—temporary nanoscale recognition between dendrons and DNA. *Org Biomol Chem* 12(3):446–455.
7. Bromfield SM, et al. (2014) Nanoscale self-assembled multivalent (SAMul) heparin binders in highly competitive, biologically relevant, aqueous media. *Chem Sci* 5:1484–1492.
8. Kala S, et al. (2014) Combination of dendrimer-nanovector-mediated small interfering RNA delivery to target Akt with the clinical anticancer drug paclitaxel for effective and potent anticancer activity in treating ovarian cancer. *J Med Chem* 57(6):2634–2642.
9. Jones SP, et al. (2011) Hydrophobically modified dendrons: Developing structure-activity relationships for DNA binding and gene transfection. *Mol Pharm* 8(2):416–429.
10. Welsh DJ, Posocco P, Pricl S, Smith DK (2013) Self-assembled multivalent RGD-peptide arrays—morphological control and integrin binding. *Org Biomol Chem* 11(19):3177–3186.
11. Bromfield SM, et al. (2014) Shape-persistent and adaptive multivalency: Rigid transgeden (TGD) and flexible PAMAM dendrimers for heparin binding. *Chemistry* 20(31):9666–9674.

12. Srinivasan J, Cheatham TE, Cieplak P, Kollman PA, Case DA (1998) Continuum solvent studies of the stability of DNA, RNA, and phosphoramidate-DNA helices. *J Am Chem Soc* 120(37):9401–9409.
13. Case DA, et al. (2014) AMBER 14 (University of California, San Francisco).
14. Pavan GM, et al. (2010) PAMAM dendrimers for siRNA delivery: Computational and experimental insights. *Chemistry* 16(26):7781–7795.
15. Karatasos K, Posocco P, Laurini E, Pricl S (2012) Poly(amidoamine)-based dendrimer/siRNA complexation studied by computer simulations: Effects of pH and generation on dendrimer structure and siRNA binding. *Macromol Biosci* 12(2):225–240.
16. Posocco P, et al. (2012) Tell me something I do not know. Multiscale molecular modeling of dendrimer/dendron organization and self-assembly in gene therapy. *Curr Med Chem* 19(29):5062–5087.
17. Andersen HC (1980) Molecular dynamics simulations at constant pressure and/or temperature. *J Chem Phys* 72(4):2384–2393.
18. Darden T, York D, Pedersen L (1993) Particle mesh Ewald: An *N*·log(*N*) method for Ewald sums in large systems. *J Chem Phys* 98(12):10089–10092.
19. Scocchi G, et al. (2009) A complete multiscale modelling approach for polymer-clay nanocomposites. *Chemistry* 15(31):7586–7592.
20. Scocchi G, Posocco P, Fermeglia M, Pricl S (2007) Polymer-clay nanocomposites: A multiscale molecular modeling approach. *J Phys Chem B* 111(9):2143–2151.
21. Keaveny EE, Pivkin IV, Maxey M, Em Karniadakis G (2005) A comparative study between dissipative particle dynamics and molecular dynamics for simple- and complex-geometry flows. *J Chem Phys* 123(10):104107.
22. Bolz RE (1973) *CRC Handbook of Tables for Applied Engineering Science* (CRC, New York).
23. Jorgensen WL, Chandrasekhar J, Madura JD, Impey RW, Klein ML (1983) Comparison of simple potential functions for simulating liquid water. *J Chem Phys* 79:926–935.
24. Liu J, Ma H, Wei T, Liang XJ (2012) CO2 gas induced drug release from pH-sensitive liposome to circumvent doxorubicin resistant cells. *Chem Commun (Camb)* 48(40):4869–4871.
25. Liu X, et al. (2014) Adaptive amphiphilic dendrimer-based nanoassemblies as robust and versatile siRNA delivery systems. *Angew Chem Int Ed Engl* 53(44):11822–11827.
26. Huang K, et al. (2012) Size-dependent localization and penetration of ultrasmall gold nanoparticles in cancer cells, multicellular spheroids, and tumors in vivo. *ACS Nano* 6(5):4483–4493.
27. Yu T, et al. (2012) An amphiphilic dendrimer for effective delivery of small interfering RNA and gene silencing in vitro and in vivo. *Angew Chem Int Ed Engl* 51(34):8478–8484.
28. Liu X, et al. (2014) Targeted delivery of Dicer-substrate siRNAs using a dual targeting peptide decorated dendrimer delivery system. *Nanomedicine (Lond Print)* 10(8):1627–1636.

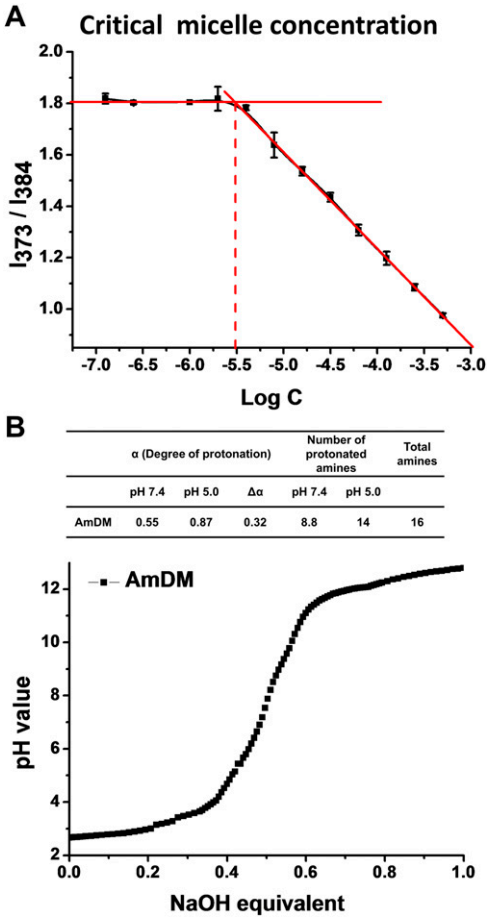

Fig. S1. (*A*) The critical micelle concentration of the amphiphilic dendrimer AmDM determined using the fluorescent dye pyrene. (*B*) Protonation state of AmDM at pH 5.0 and pH 7.4 deduced from pH titration curve of AmDM (25).

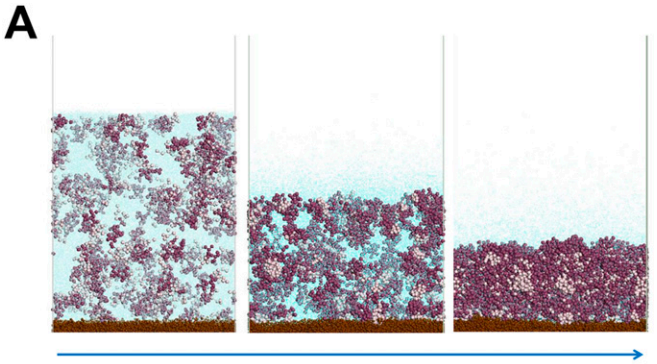

B

Optimizing drug loading content and drug encapsulating efficiency.

AmDM / DOX ratio (w/w)	drug loading content (%)	drug encapsulating efficiency (%)
15:6	30	88
15:8	37	69
15:10	42	65
15:16	40	20

Fig. S2. (*A*) Snapshots of mesoscale simulations of AmDM micelle preparation via film dispersion method at increasing simulation time (left to right). The AmDM micelles are represented in colored sticks and balls, their hydrophobic core highlighted in pink and the hydrophilic dendritic corona depicted in purple. Solvent and substrate are shown as light blue and brown spheres, respectively. (*B*) Screening the ratios of the amphiphilic dendrimer AmDM and the anticancer drug DOX for the optimal drug-loading content and drug-encapsulating efficiency.

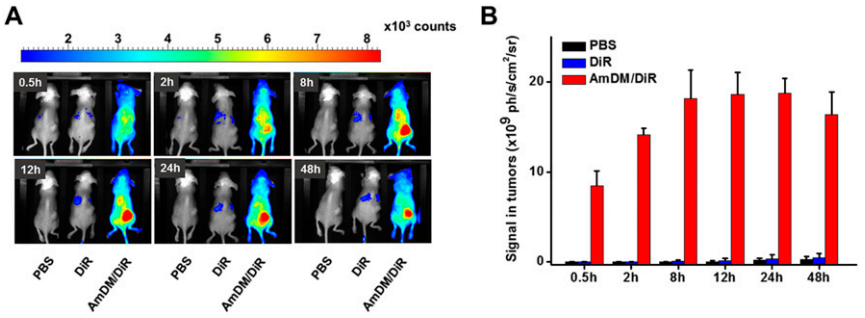

Fig. S3. Preferential accumulation of nanomicelles in tumor demonstrated using AmDM nanomicelles loaded with the near-infrared fluorescent dye DiR. NSG mice bearing MCF-7R tumors were administrated with PBS, free DiR, or AmDM/DiR via tail vein injection ($n = 4$). (*A*) In vivo images of mice after 0.5, 2, 8, 12, 24, and 48 h postinjection. (*B*) Intensity of fluorescent signal in tumors quantified after 0.5, 2, 8, 12, 24, and 48 h postinjection.

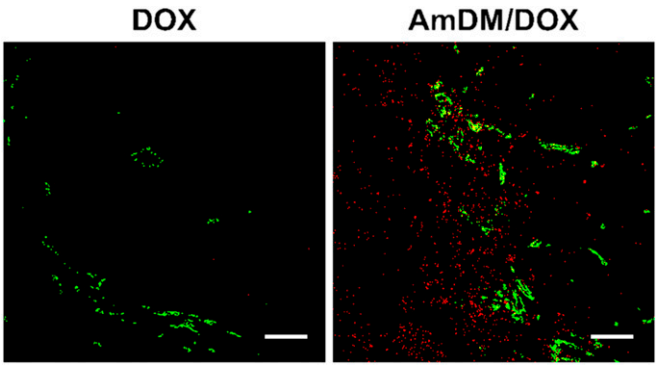

Fig. S4. Compared with the free anticancer drug DOX, AmDM/DOX nanomicelles showed significantly improved accumulation and penetration in the tumor lesion of NSG mice bearing MCF-7R tumors. Frozen sections of the tumors excised from mice 12 h posttreatment with DOX and AmDM/DOX were stained with FITC-labeled CD31 antibody to stain tumor vessels. Red signal, DOX; green signal, FITC-tagged CD31. (Scale bar: 100 μm.)

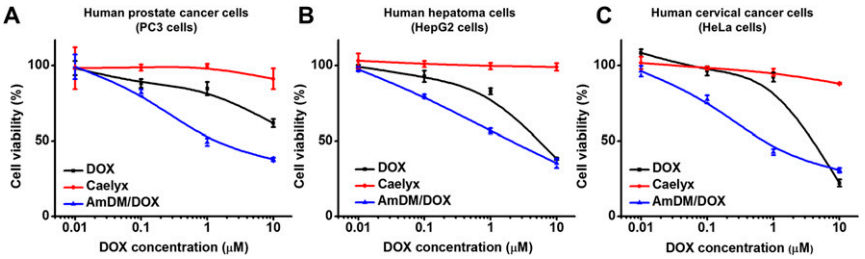

Fig. S5. Compared with the free anticancer drug DOX and the clinically used pegylated doxorubicin nanoformulation (Caelyx), AmDM/DOX nanomicelles show enhanced antiproliferation efficiency on (*A*) castration resistant human prostate cancer PC3 cells, (*B*) human hepatoma HepG2 cells, and (*C*) human cervical cancer HeLa cells. The antiproliferation activity was measured using MTT assay.

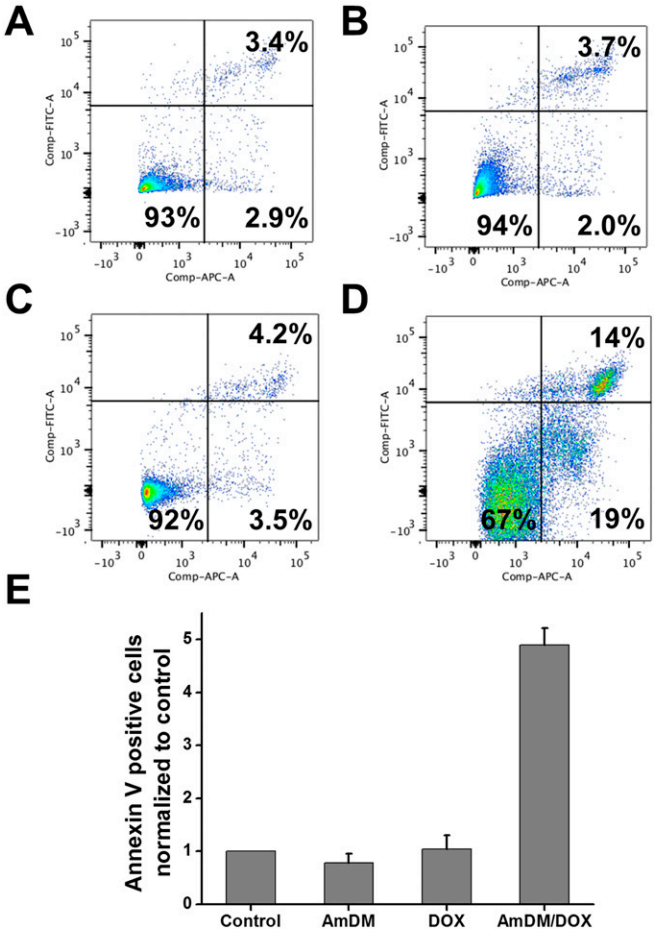

Fig. S6. Enhanced cell apoptosis was induced by AmDM/DOX nanomicelles in MCF-7R cells. Cell apoptosis assessed after treatment with (*A*) nontreatment control, (*B*) AmDM, (*C*) DOX, and (*D*) AmDM/DOX using APC Annexin V/SYTOX Green Dead Cell Apoptosis Kit. (*E*) Quantitative analysis of Annexin V positive cells after treating with nontreatment control, AmDM, DOX, and AmDM/DOX.

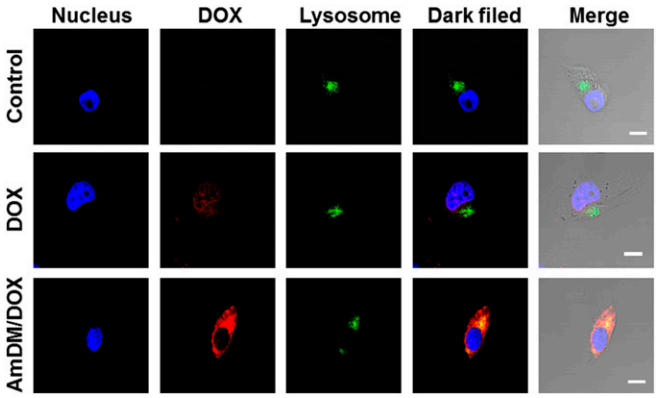

Fig. S7. AmDM/DOX micelles were partly colocalized with lysosomes in MCF-7R cells. (Scale bar: 10 μm.) MCF-7R cells were treated with DOX and AmDM/DOX at a doxorubicin concentration of 10 μM for 4 h, with nontreatment as control. LysoSensor Green was used to stain lysosomes; Hoechst 34580 was used to stain nucleus. Blue signal: nuclei; green signal: lysosomes; red signal: doxorubicin.

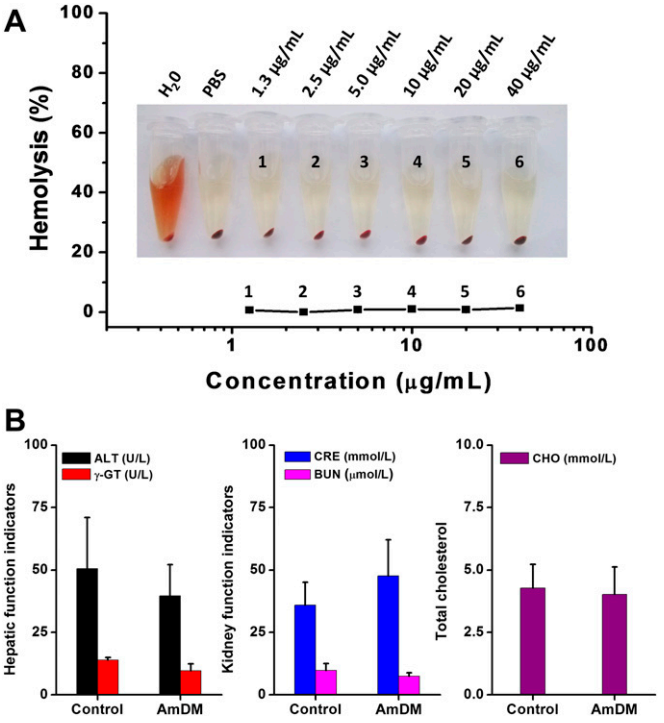

Fig. S8. Neither blood hemolysis nor dysfunction of the major organs in mice was detected after treatment with the empty AmDM nanomicelles. (*A*) No hemolytic effect was observed with red blood cells after treated with AmDM nanocarriers at varying concentrations from 1.3 to 40 μg/mL, using water as a positive control and PBS buffer as a negative control. (*B*) No notable toxicity was detected in male C57BL/6 mice treated with of AmDM (15 mg/kg) via i.v. administration, compared with PBS control. The in vivo toxicity of the AmDM nanocarrier was examined by measuring the hepatic and kidney function and the cholesterol (CHO) level in the blood via different indicators, including alanine transferase (ALT), gamma glutamyl transferase (γ-GT), creatinine (CRE), blood urea nitrogen (BUN), and cholesterol (CHO) (25).

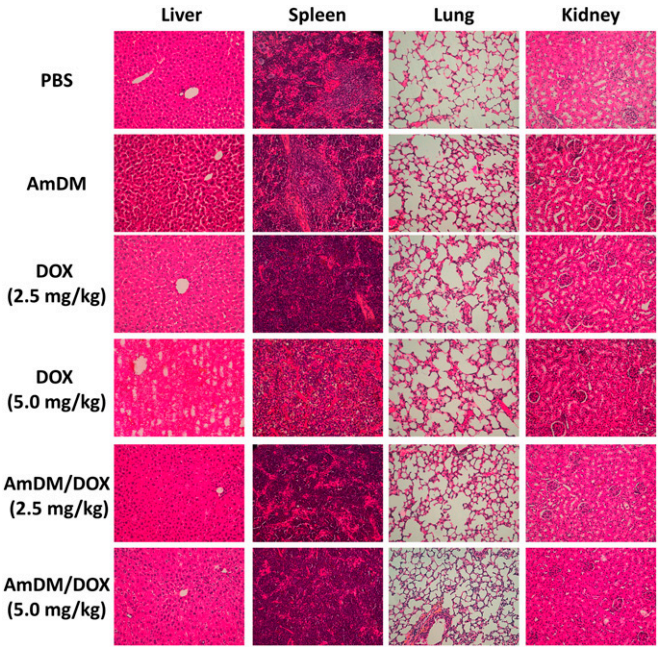

Fig. S9. Histological analysis of tissues from major organs of female NSG mice after treatment with PBS, AmDM, free DOX (2.5 and 5.0 mg/kg), and AmDM/DOX nanomicelles (2.5 and 5.0 mg/kg). The female NSG mice bearing MCF-7R were treated with PBS, AmDM, free DOX (2.5 and 5.0 mg/kg), and AmDM/DOX nanomicelles (2.5 and 5.0 mg/kg) twice per week five times. At the end, the mice were killed and all of the organs were removed for HES staining to evaluate possible toxicity. For free DOX (5.0 mg/kg), organs were taken after injection twice because of the high toxicity observed.